ELSEVIER

Journal of Molecular Structure 449 (1998) 177–201

Journal of
MOLECULAR
STRUCTURE

Matrix effects in the low-temperature ozonation of ethylene, tetramethylethylene and 1-hexene

U. Samuni[a], Y. Haas[a,*], R. Fajgar[b], J. Pola[b]

[a]*Department of Physical Chemistry and the Farkas Center for Light-Induced Processes, The Hebrew University of Jerusalem, Jerusalem, Israel*
[b]*Institute for Chemical Processes Fundamentals, The Czech Academy of Sciences, Prague, Czech Republic*

Received 26 November 1997; accepted 15 December 1997

Abstract

The ozonation of the title compounds was studied in argon and CO_2 matrices at low temperatures (12–80 K). All three were found to react with ozone in a CO_2 matrix deposited at low temperature, and having an amorphous structure. The reaction was found to start at 26 K, the temperature at which the matrix undergoes a phase transition. In contrast, only tetramethylethylene (TME) was found to react in an argon matrix, the other two compounds remaining inactive towards ozone up to the softening temperature of argon (~40 K). These results are interpreted as indicating that reaction between olefins and ozone is initiated at low temperatures once the two reactants are free to move to the required configuration. This idea is supported by molecular dynamics simulations on the TME reaction. The infrared spectra of the primary ozonide of TME, as well as of the primary and secondary ozonide of 1-hexene are reported, and compared with quantum chemical calculations. © 1998 Elsevier Science B.V.

Keywords: Ozonation; Ozonides; Olefins; Matrix isolation; Low-temperature kinetics

1. Introduction

The Criegee mechanism [1,2] is generally accepted as the best way to account for the characteristics of the ozonolysis of olefins, which leads to the cleavage of the double bond and the formation of aldehydes (or ketones) and acids. The three-step mechanism involves three intermediates, the primary ozonide, I (POZ), a carbonyl oxide (CO) + carbonyl compound, II, sometimes referred to as the Criegee intermediate (C.I.) and the secondary ozonide, III (SOZ) (Scheme 1). Recently, Cremer et al. calculated that a dipole complex should be formed between the CO and the carbonyl compound [3], this was further supported by our semiempirical calculations and comparison with experimentally found trends of ozonolysis steroselectivity of various olefins [4]. In a recent communication [5] we reported that the primary and secondary ozonides of ethylene can be formed at much lower temperatures than previously observed, and that at a given temperature the reaction's progress depends on the matrix surrounding the reacting pair. Thus, no reaction was found to take place in an argon matrix at temperatures up to 44 K, or in a crystalline CO_2 below 77 K, while in an amorphous CO_2 matrix reaction products were identified at temperatures as low as 26 K. Molecular dynamics (MD) simulations of the trapping sites of the ethylene–ozone pair in an argon matrix were reported, and it was shown that their structure is unsuitable for ozonide formation. It

* Corresponding author. Fax: 972 2 5618033

PII S0022-2860(98)00459-1

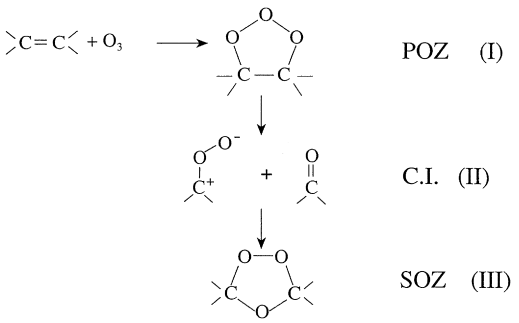

Scheme 1. An outline of the Criegee mechanism.

was postulated that the apparently more open structure [6] of low-temperature deposited CO_2 (T_{dep} = 20 K), compared with the structure of crystalline CO_2 deposited at high temperature (T_{dep} = 65 K) or to that of an argon matrix, allows the reaction to proceed at a lower temperature. However, a thermal reaction at a temperature as low as 26 K is difficult to explain in view of an estimated activation energy of 4.7–5.2 kcal/mol [7–9], for the ozonation reaction of ethylene in the gas phase and in solution. In addition, the study of ethylene ozonation at cryogenic temperatures [5] has revealed that the appearance of the two ozonide products, ethylene primary ozonide (EPOZ) and ethylene secondary ozonide (ESOZ), occurs simultaneously. Since at cryogenic temperatures EPOZ is very stable, this result was rationalized by assuming that ESOZ is formed directly from a vibrationally excited EPOZ molecule, before the latter undergoes relaxation [5].

In this paper, we extend the low-temperature study (in argon and CO_2 matrices) to two C_6 olefins—tetramethylethylene (TME) and 1-hexene, in an attempt to check the generality of our previous findings—the very low reaction temperature (26 K), the coappearance of EPOZ and ESOZ and better understand the environment effects on the reaction.

The room temperature reaction rate constants of larger olefins with ozone are bigger (e.g. by a factor of 1000 for TME) than of ethylene [9]. It is found experimentally that upon increasing chain length (for the 1-alkenes), and more importantly, the number of substituents on the double bond, the activation energy decreases (see Table 1). In a cryogenic matrix diffusion is arrested, so that a reaction is possible only between neighboring reactants (a pair) formed during deposition. A measure of the time needed to experimentally observe a reaction may be obtained by considering the half life ($\tau_{1/2}$) of the reaction between such pairs. Table 1 shows the pseudo first order rate constants at 26 K, calculated from the high-temperature parameters by assuming an effective ozone concentration of 10 M, corresponding approximately to a 1:1 ozone–olefin mixture, as well as the corresponding half lives. It is found that the reaction of TME may take place at a lower temperature range (20–40 K) during a typical experimental time interval ($\sim 10^4$ s). In this temperature range the argon matrix is still intact, thus enabling to probe the effect of the argon environment. Activation data for 1-hexene ozonolysis are not available, but extrapolation from those of the smaller olefins indicates that this reaction may also be detected over a practical time interval ($\sim 10^5$ s). In

Table 1
Kinetic data for ozonolysis of various olefins

Olefin	A[a] (cm^3/molecule/s)	Ea[a] (kcal/mol)	k_{uni} at 26 K[b] (s^{-1})	$\tau^c_{1/2}$ (s)
Ethyene	1.2×10^{-14}	5.2	2.4×10^{-36}	$2.9 \times 10^{+35}$
1-Propene	1.3×10^{-14}	4.2	6.5×10^{-28}	$1.1 \times 10^{+27}$
1-Butene	3.46×10^{-15}	3.4	9.3×10^{-22}	$7.5 \times 10^{+20}$
Cis-2-butene	3.5×10^{-15}	1.9	3.8×10^{-09}	$1.8 \times 10^{+8}$
Trans-2-butene	9×10^{-15}	2.3	4.2×10^{-12}	$1.7 \times 10^{+11}$
2-methyl-butene	6.2×10^{-15}	1.6	2.2×10^{-6}	$3.1 \times 10^{+5}$
TME	3.7×10^{-15}	0.7	4.9×10^{1}	1.4×10^{-2}

[a]The bimolecular pre-exponential factor and the activation energy for the rate constants of the ozonolysis of olefins [9].

[b]The unimolecular rate constants 26 K were computed by multiplying the bimolecular one by the concentration of ozone in a neat film consisting of a 1:1 composition of ozone and ethylene—1.01×10^{22} molecule/cm^3.

[c]$\tau_{1/2} = \ln 2/k$.

contrast, the reaction with ethylene is expected to be extremely slow and practically unobservable, if the room temperature rate parameters are valid also at cryogenic temperatures. In particular, the reaction onset is expected to be observable at a different temperature for ethylene than for TME in cryogenic matrices.

TME ozonolysis was studied by various techniques and in different phases. In neat films Heicklen et al. identified TMEPOZ bands at $T \geq 183$ K [10]. Nelander et al. studied TME and ozone in argon and in crystalline CO_2 matrices (CO_2 matrices deposited at a temperature of 65 K) [11]. In this study, relatively high concentrations (1:1:100) were used—so that the possible involvement of complexes larger than 1:1 in the reaction cannot be neglected. These workers searched for a charge transfer UV absorption band in these systems, but failed to observe any. In contrast, the more recent work of Singmaster and Pimentel, in which a careful control of the temperature was exercised, reported a charge transfer complex of TME–ozone using visible–UV absorption in krypton and argon matrices [12]. Several low-temperature gas-phase studies attempted to map out the product distribution for TME (and also 1-hexene) ozonolysis, in an effort to clarify the complete reaction mechanism [13–16].

1-Hexene ozonides were studied by Razumovskii et al. and later on by Boldenkov, the activation energy for ozonide decomposition was determined: 7 kcal/mol (± 20%) [17] for the primary ozonide (HPOZ) and 23.7 kcal/mol [18] for the secondary ozonide (HSOZ). Later on, Mile et al. investigated the infrared spectra and kinetics of decomposition of 1-hexene primary ozonide in the liquid phase at low temperatures ($\log_{10}A = \sim 3\ s^{-1}$, $Ea < 2.9$ kcal/mol) [19], which is different from the value reported by Razumovskii.

In 1-hexene low-temperature ozonation both HPOZ and HSOZ were observed, a trend typical of primary olefins [5,20]. In contrast, low-temperature TME ozonation yields only the TMEPOZ which dissociates to the final end products at higher temperatures. The absence of TMESOZ was accounted for within the framework of the Criegee mechanism by assuming that the ketone formed from TMEPOZ is inert towards reaction with the carbonyl oxide, preventing the retro-cycloaddition step and TMESOZ formation [10,20,21]. Recently, Griesbaum et al. have succeeded synthesizing TMESOZ by the indirect method of ozonation of O-methyl oxime of acetone and later detected TMESOZ (though in minute amounts) in the ozonolysis of TME on polyethylene. They found that TMESOZ is a very stable molecule and characterized it by NMR, IR and CI-MS spectroscopies [22,23].

Previous cryogenic studies of the ozonolysis reactions were aimed mostly at identifying reactive intermediates and did not explicitly consider the effect of site structure—possible environmental influence on the reaction's feasibility and progress rate. In particular, the high concentration of reactants used may have led to reactions within large reactant's clusters, perhaps obscuring matrix effects. In this study, an effort was made to work with the highest dilution that still enabled the detection of products, thus, contrary to the majority of previous matrix studies, making it easier to follow the specific role of different matrix environments. In this paper we report experiments designed to assess influence of the solid environment on the reaction feasibility and progress as well as preliminary attempts to correlate the data with computer simulations of site structure.

2. Experimental and computational details

Ozone was prepared from a purified oxygen (98.5%, main impurity N_2) by electric discharge. Ethylene (99.5%) from Aldrich, 1-hexene (99%) from Aldrich, tetramethylethylene (TME) (98%) from Fluka, argon (99.9999%) from Matheson, CO_2 (99.6%) from Gordon-Gas, were all used as received. Each gas was mixed separately with a carrier gas (argon or CO_2) to the desired concentration using standard manometric techniques. The gases were co-deposited (at a rate of 2–10 mmol/h) from two different gas lines on a KBr window attached to the cold tip of a closed cycle helium cryostat (Air Products model CS202). A stainless steel line was used for the olefins and an all-glass vacuum line was used for ozone to reduce ozone decomposition during deposition. The infrared spectrum of the resulting matrix was recorded by a Fourier transform spectrometer (Nicolet model 520, 0.5 cm^{-1} resolution) at any desired temperature higher than 12 K.

The temperature was controlled by a Lake Shore Cryogenics Temperature Controller (model 330 Autotuning) to within ± 0.5 K. Three characteristic temperatures were used in the experiments: T_{dep}, the deposition temperature; T_{reac}, the reaction temperature; and T_{spec}, the temperature at which the spectrum were recorded. Typically, the matrix temperature was raised gradually, the temperature at which new product bands first appeared in the IR spectra is referred to as T_{reac}. The matrix was left at the reaction temperature for periods varying between a few minutes and several hours.

Amorphous CO_2 matrices were prepared by using T_{dep} = 20 K or lower. It was claimed that for CO_2 [24–26], deposition in the temperature range of 15–30 K leads to the formation of an amorphous solid, while careful deposition at temperatures higher than 55 K results in a cubic T_{6h} crystalline structure. The amorphous form is characterized by the appearance of 'forbidden' molecular transitions of CO_2, ν_+ and ν_- (1384.5 and 1279 cm^{-1}, respectively), which are believed to be induced in the solid by a non symmetric structure [24–26]. Under these deposition conditions the resultant solid has a very high surface area as determined from H_2 absorption [6,27] experiments. It should be noted that minor impurities in the CO_2 gas may be important to the formation of the amorphous matrix. Thus, Knozinger et al. [6] reported, based on X-ray powder diffraction, the formation of polycrystalline CO_2 matrix when using ultra clean (99.995%) CO_2 gas even at low deposition temperature, 20 K (though, at these conditions they also reported a high specific surface area, 210 m^2/g and in addition the X-ray technique is only sensitive to ordered structure). Depositions in mixed solvent were done by pre-mixing CO_2 and argon to the desired ratio; all other deposition conditions (such as deposition temperature and deposition rate) were the same as those used to generate the amorphous neat CO_2 matrix.

In all experiments, the appearance and subsequent growth of new bands in the infrared spectrum was the indication that reaction took place. The assignment of the spectra was aided by an ab-initio calculation of the vibrational frequencies and infrared intensities of the relevant POZ and SOZ products. Ab-initio calculations were carried out using the Gaussian 94 (and Gaussian 92) program package [28], at the HF or HF-MP2 levels and by the density functional theory at the B3LYP level. Several basis sets were used, the largest of which was 6-311G* [29]. Complete structural optimization was performed for each species and vibrational frequencies were calculated from the Hessian matrix using the harmonic approximation at the optimized geometry. No imaginary frequencies were found in the calculation, showing that the optimized structure was indeed a minimum. The resulting frequencies were uniformly scaled for the HF-MP2/6-31G calculation by 0.9338 or 0.9613 for the B3LYP/6-311G* [30].

Molecular dynamics simulations were performed as previously described [31], except that the molecules

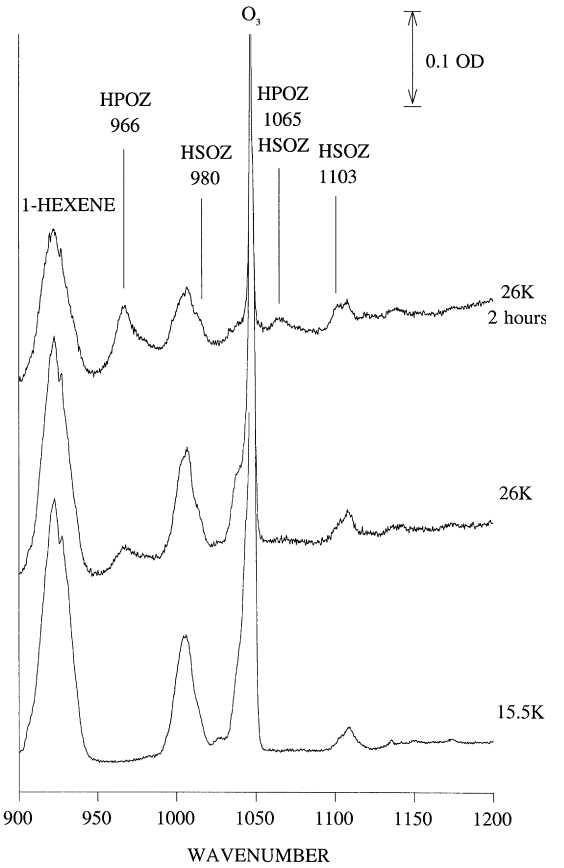

Fig. 1. IR spectra of 1-hexene and ozone in an amorphous CO_2 matrix (1-hexene:ozone:CO_2 1:1:700; T_{dep} = 15.5 K) Bottom: just after deposition at 15.5 K. Middle: after heating the matrix to 26 K. Top: after 2 h at 26 K.

Table 2
Rate constants of ethylene and TME ozonide formation in amomphous CO_2 matrix

Exp.	Matrix composition	Ozonide	IR band (cm^{-1})	Temperature (K)	k_{uni} (min^{-1})
1	ethylene:ozone:CO_2 1:1:580	ESOZ	1072	25	$(1.4 \pm 0.6) \times 10^{-3}$
2	ethylene:ozone:CO_2 1:1:580	ESOZ	1072	26.5	$(2.6 \pm 0.8) \times 10^{-3}$
3	TME:ethylene:ozone:CO_2 1:1.12:2:600	ESOZ	1072[a]	26.5	$(1.06 \pm 0.03) \times 10^{-2}$
3	TME:ethylene:ozone:CO_2 1:1.12:2:600	TMEPOZ	1143[b]	26.5	$(1.05 \pm 0.08) \times 10^{-2}$
3	TME:ethylene:ozone:CO_2 1:1.12:2:600	TMEPOZ	1200	26.5	$(8.1 \pm 0.5) \times 10^{-3}$
4	TME:ozone:CO_2 1:1:620	TMEPOZ	1200	25	$(3.9 \pm 0.4) \times 10^{-3}$

[a]See Fig. 6(a).
[b]See Fig. 6(b).

were treated as rigid bodies using the RATTLE algorithm [32]. The geometry of the molecules used in the MD simulations was taken either from microwave experimental data or, when these were not available such as for TMEPOZ, from ab initio calculations (MP2/6-31G for TMEPOZ). Different trapping sites could be generated in different runs, and the most frequently encountered ones were considered the most stable ones, as discussed in more detail elsewhere [31].

3. Results

3.1. Ozonation in low-temperature deposited CO_2 matrices

1-Hexene and ozone were found to react in an amorphous CO_2 matrix at temperatures as low as 26 K. Fig. 1 shows a portion of the IR spectra of 1-hexene and ozone in an amorphous CO_2 matrix. Warming the matrix to 26 K brought about a decrease of the ozone and 1-hexene bands and the appearance of new bands. These bands belong to HPOZ and HSOZ based on literature data [19], on our neat film results and supported by ab initio calculations (see Table 2, Table 3). After 2 h at 26 K, there was further decrease in the reactants bands and increase of the products bands.

TME and ozone deposited in an amorphous CO_2 matrix (T_{dep} = 12.5 K) did not react at temperatures lower than 25–26 K. At that temperature new bands assignable to TMEPOZ [10] appeared and continued to increase reaching a plateau after 14 h (Fig. 2).

For both olefins (as was the case with ethylene ozonation [5]), no IR bands owing to either POZ or SOZ were observed, even for elongated periods of time (several days), as long as the matrix was kept at temperatures below 25 K.

3.2. CO_2 matrix crystallization process

Another significant change that occurred during heating of the low-temperature deposited CO_2 matrix is the decrease of the CO_2 ν_+ and ν_- bands (1384.5 and 1279 cm^{-1}, respectively) [24–26]. This decrease is clearly seen in Fig. 2. It was observed for all low-temperature deposited CO_2 matrices, even when only one component (or none) was introduced to the matrix. We noted that in all these matrices the changes started only at the temperature range of 25–26 K. Fig. 3 demonstrates this for an amorphous CO_2 matrix containing only ozone as a guest, namely, when ozonation does not take place. It can be seen that below 26 K there is a negligible decrease of the molecular forbidden bands of CO_2 (ν_+, ν_-), but upon heating to 26.5 K a rapid decrease sets in: within 30 min the peak's area decreased by 30%.

3.3. Ozonation in argon matrices

TME and ozone reacted in an argon matrix at temperatures as low as 30 K. Fig. 4 shows a portion of the IR spectrum of TME and ozone in an argon matrix. Examination of the lowest trace, taken just after deposition (at T = 12.5 K), shows that it already contains weak bands of TMEPOZ probably owing to some reaction during deposition. Raising the matrix temperature up to 30 K does not lead to any detectable spectral changes. At that temperature a gradual increase of TMEPOZ bands and a decrease of the TME bands is clearly observable. The matrix was

Table 3
The experimental and calculated vibrational frequencies of HPOZ

Exp. frequency[a] (cm^{-1})	Exp. frequency[b] neat film (cm^{-1})	Exp. intensity[b] neat film (a.u.)	Calc. frequency[c] (cm^{-1})	Calc. intensity[c] (km/mol)
692	648	30	668	7.2
	691	3	688	3.9
725	722	29	704	15.8
740	739	26	713	21.9
	793	9	771	2.2
	843	15	826	2.8
	848	15	868	3.8
			882	2.5
			905	2.5
975	963	100	946	39.5
			975	0.3
			982	0.9
1001	1004	4	999	1.3
			1025	0.5
	1066	16	1052	4.0
	1118	6	1105	3.2
	1149	1	1141	0.4
			1191	0.3
	1208	2	1211	1.0
1230	1227	8	1238	0.9
	1235	3	1272	0.2
1275	1274	5	1288	0.7
			1298	0.2
	1316	3	1305	2.8
	1334	4	1322	1.4
	1372	18	1353	8.4
			1361	2.2
	1389	5	1375	4.7
			1441	0.7
			1446	1.1
			1457	1.4
			1460	8.7
			1462	1.1
	1470	133	1469	9.9
	2841	5	2886	9.2
	2858	93	2899	25.8
			2906	0.4
	2871	49	2908	18.6
	2895	7	2909	37.6
	2913	20	2917	38.6
			2928	17.5
	2929	131	2931	56.9
			2955	30.9
	2949	127	2967	93.2
	2967	75	2972	47.4
			2995	28.1

[a]Experimental vibrational frequencies [19].

[b]Experimental vibrational frequencies in a neat film—this work. Intensity determined from the area of the vibrational bands in a neat film, and normalized to the strongest band in the finger print region. Note that the 1470 cm^{-1} band is wide, corresponding to several calculated frequencies (in the region 1460–1470) which explains the seemingly mismatch of intensities. In addition, the bands in the 2800–3000 cm^{-1} region of the experimental spectra are broad and overlapping causing significant uncertainty in the determination of the area if individual bands.

[c]Calculated vibrational frequencies, (B3LYP/6-311G*, factor of 0.9613).

maintained at the same temperature for elongated periods of time, until the product bands intensity reached a constant value. In this matrix, raising the temperature further (for instance to 35 K) yielded an additional increase in the product bands intensity (see Fig. 4), showing that the plateau reached at the lower temperature did not represent complete exhaustion of the reaction potential in the matrix under diffusion-limited conditions. At 40 K a sharp increase of the product bands (and a decrease of those of the reactants) is observed. At this temperature the argon matrix softens, and translational motion of trapped species becomes possible. This finding is in accord with the report of Nelander et al. of TME ozonation in an argon matrix upon heating to 40 K [11].

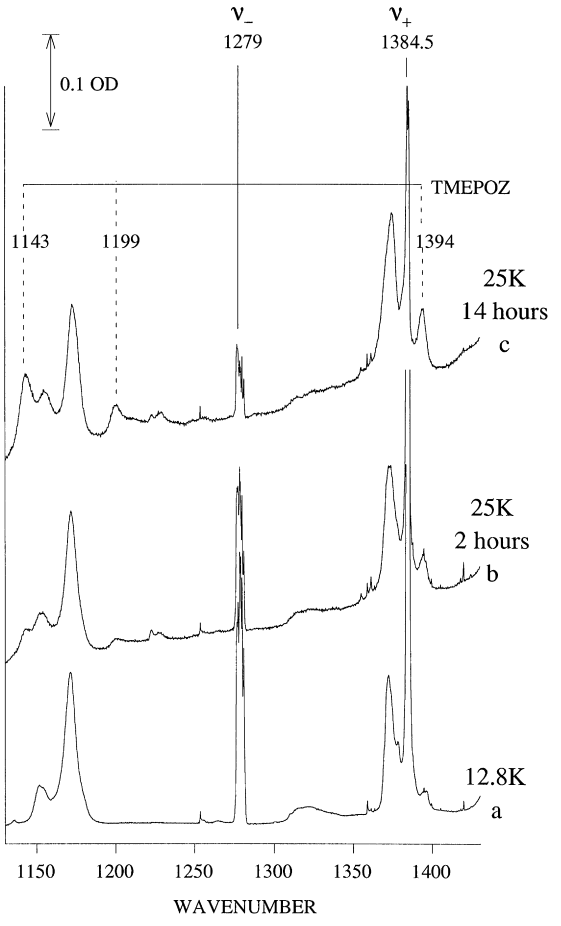

Fig. 2. IR spectra of TME and ozone in an amorphous CO_2 matrix (TME:ozone:CO_2 1:1:620; T_{dep} = 12.8 K). (a) Just after deposition at 12.8 K; (b) after 2 h at 25 K; (c) after 14 h at 25 K.

In contrast with the above TME results, no reaction between 1-hexene and ozone in an argon matrix could be detected below 40 K. When the temperature was raised above 44 K, product bands appeared conspicuously (as in the case of ethylene [5]). At this temperature the vapor pressure of argon is high enough for the matrix to be quickly pumped away, and the infrared spectra of the remaining species was found to contain a mixture or unreacted reactants (1-hexene and ozone) and of the HPOZ and HSOZ, as determined by comparison with previously published spectra [19] and ab initio calculated frequencies (see Tables 2 and 3).

3.4. Ozonation of a 1:1 mixture of ethylene and TME in amorphous CO_2 matrix

Fig. 5 shows a portion of the IR spectra of a codeposition of TME and ethylene with ozone in a CO_2 amorphous matrix. Upon warming the matrix to 26 K new bands assignable to both ethylene ozonides and TMEPOZ appear. Warming to a lower temperature than 26 K did not bring about any increase of TME ozonation products bands in spite of its lower gas-phase activation energy (compared with ethylene

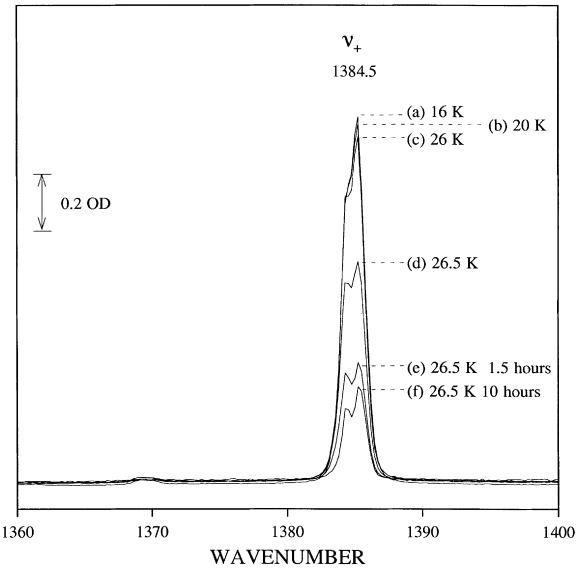

Fig. 3. IR spectra of a low-temperature deposited CO_2 matrix (O_3:CO_2 1:310; T_{dep} = 15 K). (a) Just after deposition at 15.5 K; (b) at 20 K; (c) just after heating to 26 K; (d) at 26.5 K, 30 min from first warming to 26 K; (e) after 1.5 h at 26.5 K; (f) after 10 h at 26.5 K.

ozonolysis, see Table 1). Rather, both TME and ethylene ozonides first appear only at 26 K. Fig. 6 compares the rate of formation of TMEPOZ and ethylene SOZ at 26.5 K in a CO_2 amorphous matrix (TME:ethylene:ozone:CO_2 1:1.12:2:600) by monitoring the area of their strongest bands (1143 cm^{-1} for TMEPOZ and 1072 cm^{-1} for ESOZ). In order to convert the values from optical density to concentration one needs the molar extinction coefficients (the initial concentration of reactants being the same and the optical path-length being identical since both are in the same matrix). Unfortunately, these coefficients are not available. A rough estimate of the extinction coefficients ratio was obtained from an ab initio calculation (MP2/6-31G) of the vibrational frequencies and IR intensities of these ozonides: 30 and 170 km/mol for the two bands, respectively. Thus, optical densities were converted to concentrations by dividing the experimental OD by the calculated IR intensity. The validity of this estimate was checked by comparing the TMEPOZ concentration determined from two different TMEPOZ IR bands: 1143 and 1200 cm^{-1}; the resulting concentrations were equal to within 10% (the area of the 1200 cm^{-1} band was divided by a calculated IR intensity of 6 km/mol). The resulting changes in relative concentrations with time are shown in Fig. 6. It is found that at 26.5 K the TMEPOZ's rate of formation is much faster than that of ESOZ (by a factor of ~30). Note that the matrix was kept at 25 K for about 2 h before beginning the 26.5 K experiment, resulting in the appearance of weak

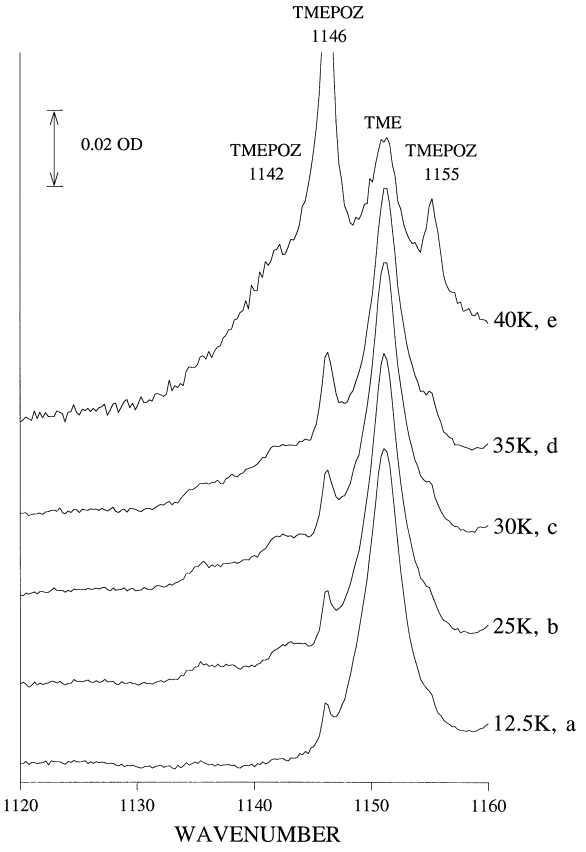

Fig. 4. IR spectra of TME and ozone in an argon matrix (TME:ozone:Ar 1:1:650; T_{dep} = 12.5 K). (a) Just after deposition at 12.5 K; (b) after 11.5 h at 25 K; (c) after 7 h at 30 K; (d) after 30 min at 33 K; (e) after 40 min at 40 K.

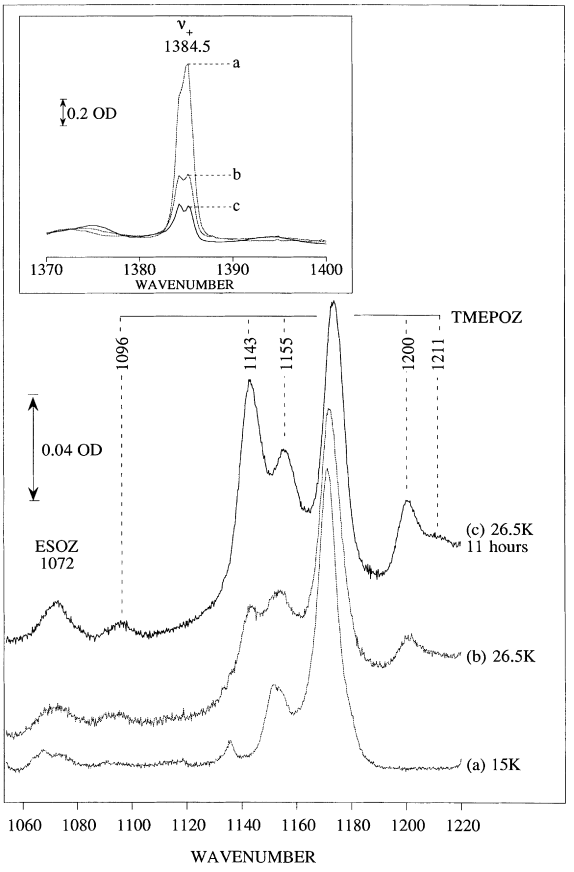

Fig. 5. IR spectra of TME, ethylene and ozone in a amorphous CO_2 matrix (TME:ethylene:ozone:CO_2 1:1.12:2:600; T_{dep} = 15 K). (a) Just after deposition at 15 K; (b) just after heating to 26.5 K; (c) after 11 h at 26.5 K. The insert shows the change in the ν_+ CO_2 band, under the same conditions.

product absorption bands, which account for the finite product concentration at time zero in Fig. 6.

The calculated curves shown in Fig. 6 assume pseudo first order kinetics. For the two curves shown in the Figure, the rate constant is found to be $(1.05 \pm 0.08) \times 10^{-2}$ min^{-1}. It follows that while the rate of formation of TMEPOZ is much larger than that of ESOZ, the rate constants of the reactions are practically identical. Converting these rate constants back to a bimolecular rate constant, using an effective ozone concentration of 10 M as in Table 1, we get $k = 2.8 \times 10^{-25}$ cm^3/molecule-s, 11 orders of magnitude smaller than the rate extrapolated from the high-temperature data for ethylene, and 26 orders of magnitude larger than the rate extrapolated from the high-temperature data for TME. Table 2 compares the pseudo first order rate constants for ethylene or TME ozonation in several separate experiments. It can be seen that although there is some scatter in the data all values are similar, within an order of magnitude, and there is no obvious trend with temperature or olefin indicating that within the experimental error the rate constants are the same. In conclusion, even though the number of data points in Fig. 6 is too small for an accurate determination of the rate constants, evidently the simple extrapolation from the high-temperature rate parameters obtained in fluid media is not appropriate.

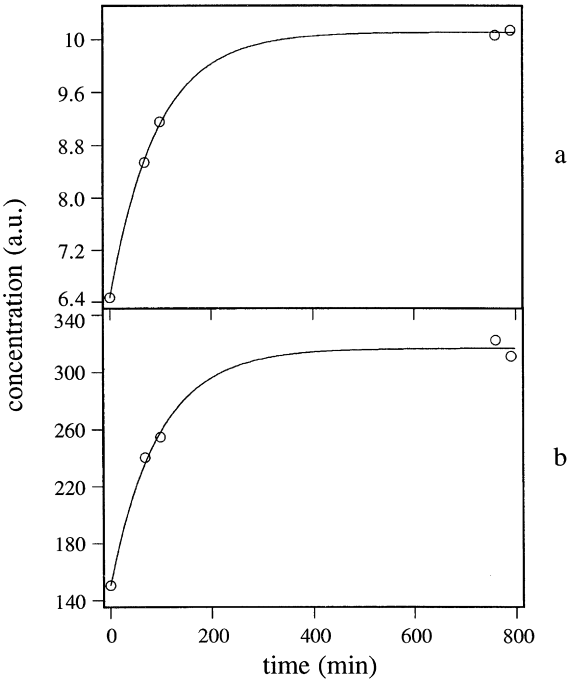

Fig. 6. The rate of formation of TMEPOZ and ESOZ at 26.5 K in a CO_2 amorphous matrix (TME:ethylene:ozone:CO_2 1:1.12:2:600). See text for the method used to convert IR intensities to concentrations. (a) ESOZ (1072 cm^{-1} band); (b) TMEPOZ (1143 cm^{-1} band). The curves are calculated assuming pseudo first order kinetics, yielding the rate constants listed in Table 2. The fit quality was good: $R^2 = 0.999$ and 0.995, respectively.

3.5. Ozonation of ethylene in mixed matrices

The fact that the reaction is observed in amorphous CO_2 at temperatures as low as 25–26 K suggests the use of this porous 'solvent' for the quantitative study of the kinetics of reactions characterized by low activation barriers. Quantitative estimates of the rates in amorphous CO_2 were hampered by its tendency to be fragile under the conventional preparation scheme used in this work. In an attempt to prepare a mechanically more stable matrix while maintaining the low-temperature reaction, mixed matrices were made up of CO_2 and argon in varying proportions. In most of these experiments the olefin used was ethylene.

It was found that the location and shape of the reactants (ethylene and ozone) IR bands strongly depended on the matrix composition. Fig. 7 shows the IR spectra in the region of the ν_7 band of ethylene (left side) and the ν_3 band of ozone (right side) in different matrices. The ozone ν_3 band was centered at 1039.7 cm^{-1} in argon and at 1048.1 cm^{-1} in the CO_2. The ethylene ν_7 band was at 947.3 cm^{-1} in argon and at 969.5 and 946 cm^{-1} in the CO_2 matrices. The forbidden CO_2 molecular bands, ν_+ and ν_-, were observed in all of the prepared mixed matrices. When the CO_2 content was less than 90%, no reaction was observed even upon heating up to 35 K and leaving the matrix overnight. Upon warming the 1:9 Ar/CO_2 mixture (ethylene:O_3:solvent 1:1:700) to 26 K the ν_+ and ν_- lines decreased and new product bands appeared and increased with time (Fig. 8).

Again it is noted that both processes begin only at 26 K and not at a lower temperature. In the 1:1 Ar:CO_2 (O_3 dilution 1:400 ethylene dilution 1:1800) mixed matrix the ν_+ and ν_- lines are also present, however they remain unchanged at 26 K. Moreover, no new product bands could be detected (heating to 32 K and maintaining the matrix at that temperature

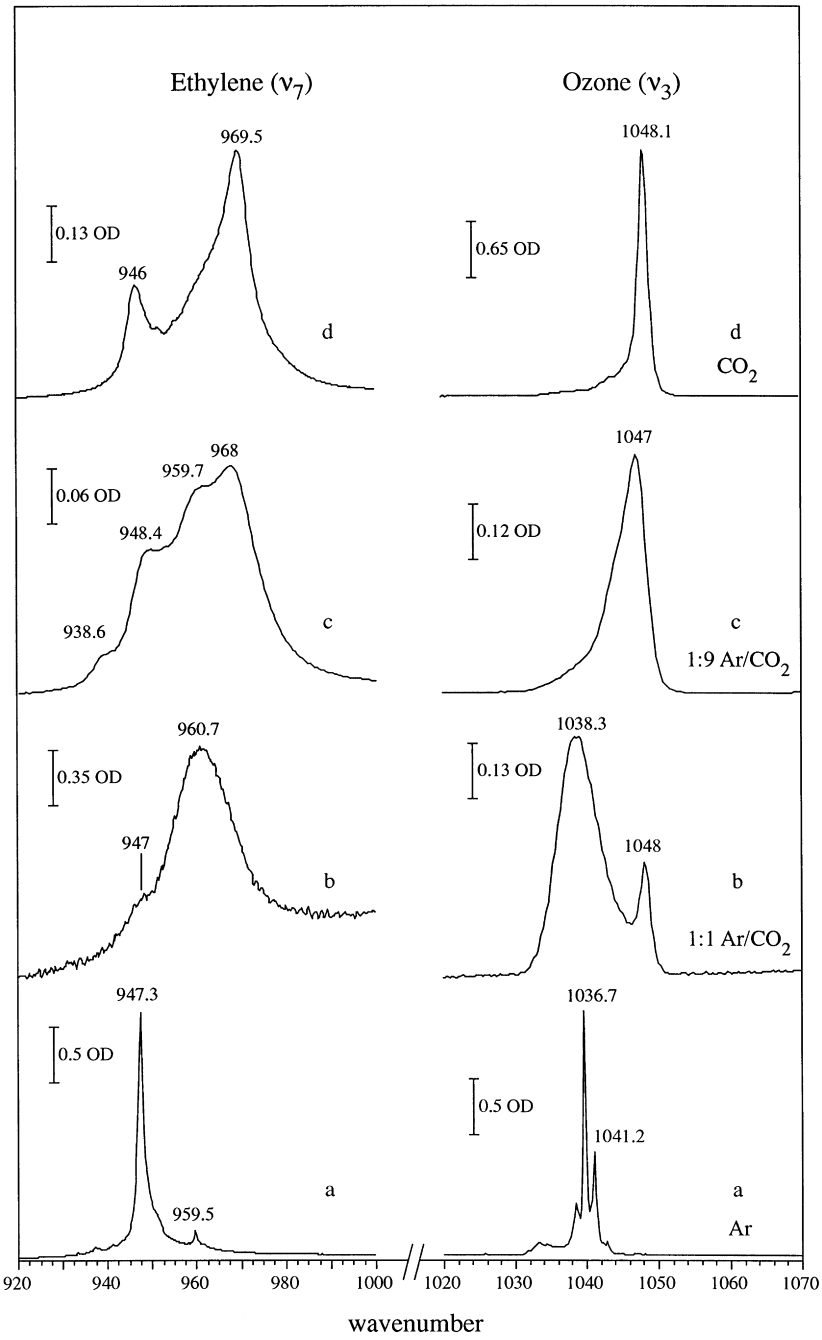

Fig. 7. The IR spectra in the region of ethylene's ν_7 band and ozone's ν_3 band in different matrix compositions. (a) Ethylene:ozone:argon 1:1:630, T_{dep} = 15 K; (b) ethylene:ozone:solvent 1:5:2000, solvent mixture is Ar:CO_2 1:1, T_{dep} = 18 K; (c) ethylene:ozone:solvent 1:1:700, solvent mixture is Ar:CO_2 1:9, T_{dep} = 17 K; (d) left side is ethylene:CO_2 1:280, T_{dep} = 15 K; right side is ozone:CO_2 1:300, T_{dep} = 20 K.

overnight also lead to no decrease of the ν_+ and ν_- lines nor to any product formation). Attempts to induce a reaction between ozone and 1-hexene in mixed matrices (8:2 Ar:CO_2 and 9:1 Ar:CO_2) in the 26–35 K temperature also did not lead to product formation.

4. Data analysis

4.1. Vibrational spectra of the product ozonides

4.1.1. HPOZ and HSOZ bands in a neat film

The infrared spectra of HPOZ and HSOZ were recorded in a neat film experiments. Bands due to a given species were assigned by monitoring the rate of their increase and then decrease as a function of time at the following temperatures: 120, 150, 170, 180 and 220 K. At these temperatures the reactants 1-hexene and ozone evaporate and thus ambiguity in the assignment owing to overlap with the product bands is eliminated. Fig. 9 shows the IR spectra of a 1-hexene and ozone mixture in an argon matrix. Just after deposition at 15 K and then at increasingly higher temperatures the gradual disappearance of the reactant bands (owing to reaction and evaporation), the appearance of product bands (primarily HPOZ) at 120 and 150 K and finally at 170 K the disappearance of HPOZ bands and increase of HSOZ bands.

To assist in the product bands assignment we performed ab initio calculations of HPOZ and HSOZ vibrational frequencies. Table 3 shows a comparison of experimental and calculated vibrational frequencies of HPOZ. The tentative assignment (in the absence of any isotopic data) was helped by considering both the calculated frequency and IR intensities. Agreement between calculated and experimental frequencies is seen to be reasonably good. Calculations were performed at different levels of theory, the most extensive ones being MP2-6-311G* and B3LYP/6-311G*.

These calculations yielded also the optimized geometry of HPOZ, for which experimental data are not yet available. The structure obtained by a DFT (B3LYP/6-311G*) calculation, shown in Scheme 2 indicates that the five-membered ring (COOOC) is nearly of C_S symmetry, similar to the experimentally reported one for EPOZ [33] which was also by obtained computationally [34].

Table 4 shows that the experimental spectrum of HSOZ also agrees well with the calculated one. Scheme 3 shows the calculated geometry of HSOZ (B3LYP/6-311G*). The structure of the five-membered ring (COOCO) is nearly of C_2 symmetry, similar to that reported for ESOZ, as found experimentally [35,36] and in calculations [34]. The calculations, thus, support the notion that the ozonides of primary olefins (i.e. having a terminal CH_2 group) have a similar ring structure as ethylene ozonides.

4.1.2. TME ozonide bands

The IR spectra of TMEPOZ were recorded in an argon matrix (Table 5), a CO_2 matrix and in a neat film. The peaks were assigned to a given single

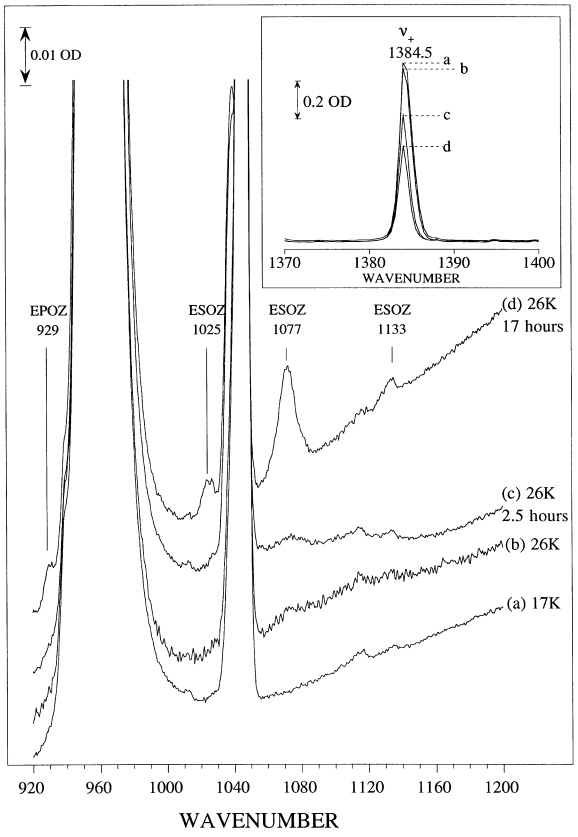

Fig. 8. IR spectra of ethylene and ozone in a low-temperature deposited mixed matrix (dilution ethylene:ozone:solvent 1:1:700; solvent-mixture is: Ar:CO_2 1:9; T_{dep} = 17 K). (a) Just after deposition at 17 K; (b) just after heating to 26 K; (c) after 2.5 h at 26 K; (d) after the 17 h at 26 K. The insert shows the spectral region of the forbidden CO_2 molecular transitions, ν_+/ν_-.

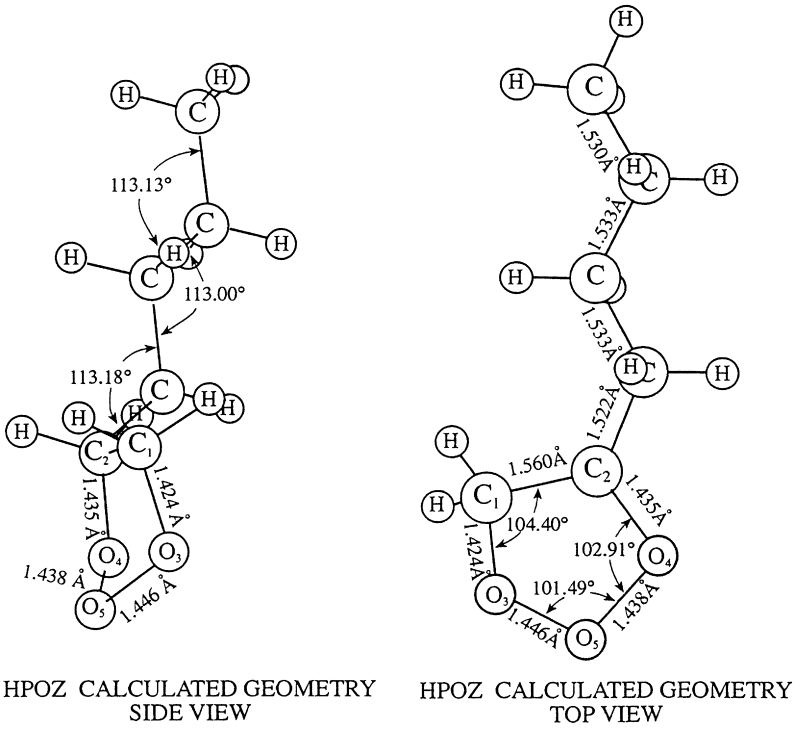

Scheme 2. The calculated structure of the primary ozonide of 1-hexene.

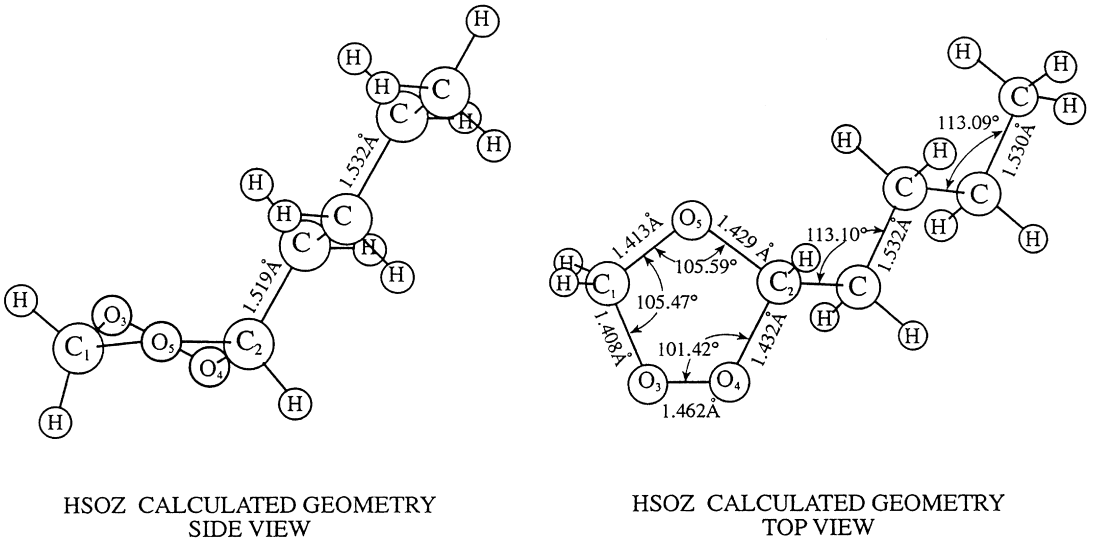

Scheme 3. The calculated structure of the secondary ozonide of 1-hexene.

chemical species by monitoring their simultaneous change with time as a function of temperature. None of the peaks that appeared in matrices containing TME and ozone, or upon TMEPOZ decomposition could be identified with the TMESOZ frequencies reported by Griesbaum et al. [23] or with those obtained by our ab initio calculations (see Table 6). Thus, TMESOZ is not formed in argon or CO_2 matrices nor in a neat film.

As in the case of HSOZ and ESOZ, TMESOZ calculated geometry is found to be of C_2 symmetry (see Scheme 4). However, TMEPOZ geometry is calculated to be of C_2 rather than C_S symmetry found for primary ozonides (Scheme 5). The twisting of the five member ring (COOCO) to a C_2 symmetry helps to minimize the repulsion between the four methyl groups, as can be seen from the side view. Table 7 lists the geometry, dipole moment, rotational constants, geometry and energy of TMEPOZ calculated using several methods and basis sets. The main difference between the simple HF calculation and the more extensive MP2/4-31G and MP2/6-31G ones involved the O–O–O ring. This result is expected since a proper description of the O–O–O moiety should include correlation effects. Interestingly, the AM1 calculation resulted in TMEPOZ of C_S geometry, similar to that of EPOZ. Other main differences of this calculation (compared with the rest of the calculations) are in the O–O–O angle (by 4°) and in the O–O bond (by -0.28 Å). To verify that TMEPOZ equilibrium geometry is indeed of C_2 rather than C_S symmetry, the calculation was repeated

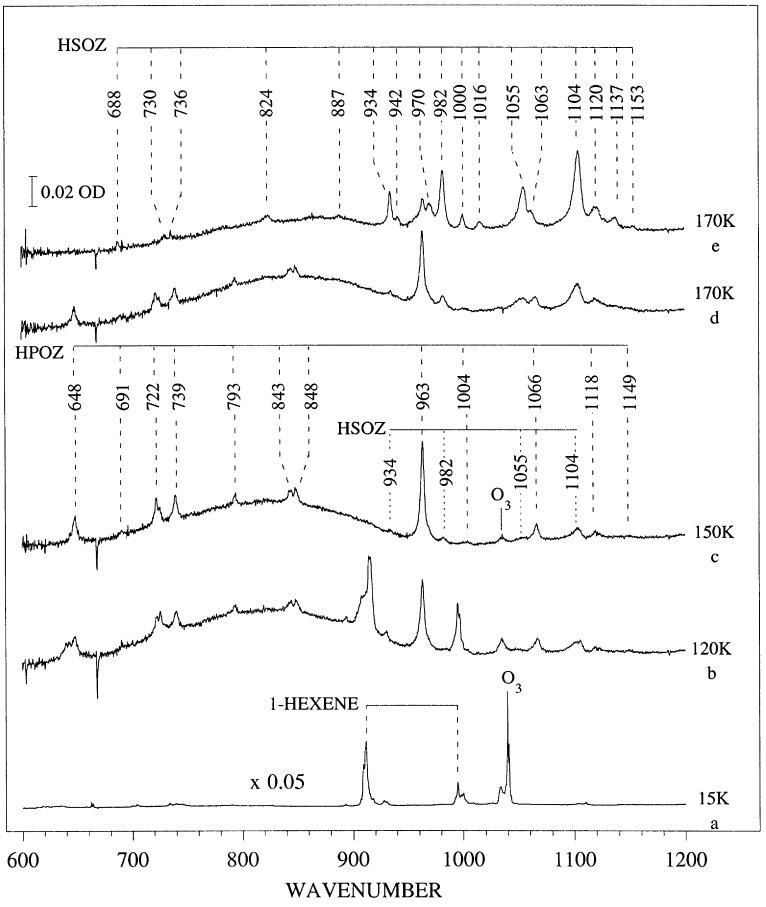

Fig. 9. IR spectra of 1-hexene:ozone:Ar 1.5:1:815 matrix. (a) Just after deposition at 15 K; (b) after 1 h at 120 K; (c) just after heating to 150 K; (d) just after heating to 170 K; (e) after 3.7 h at 170 K. (Spectra (b)–(e) are in a neat film since the argon solvent has evaporated.)

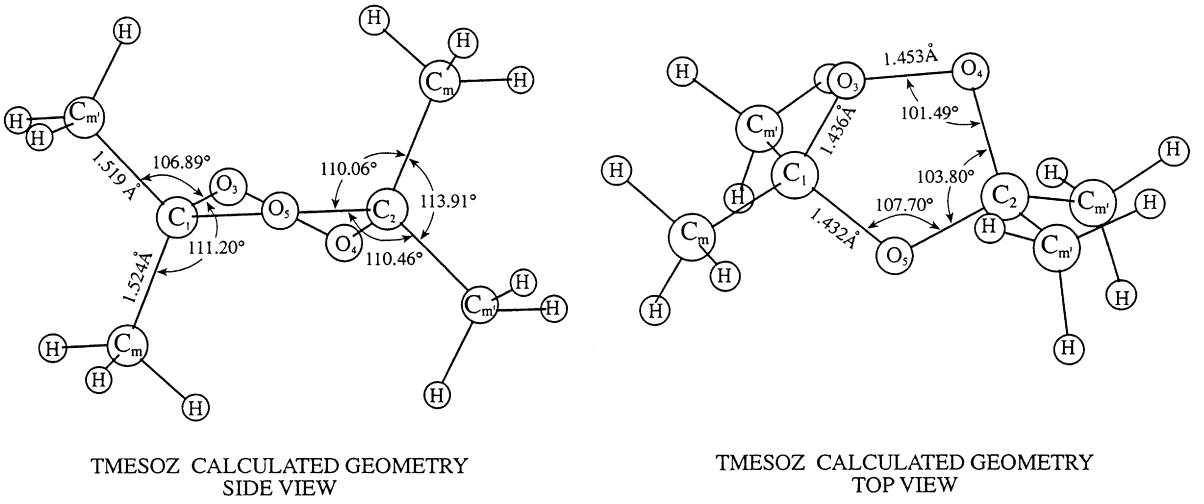

TMESOZ CALCULATED GEOMETRY
SIDE VIEW

TMESOZ CALCULATED GEOMETRY
TOP VIEW

Scheme 4. The calculated structure of the secondary ozonide of tetramethylethylene.

(using high level methods and large basis sets) starting with the AM1 optimized geometry of TMEPOZ (of C_S symmetry). In all instances the calculation's optimization procedure lead to a final geometry of C_2 symmetry.

It is interesting to note that the calculations involving basis sets with polarization functions (such as 6-31G* or 6-311G*) failed to reach an optimized bound structure for TMEPOZ; rather, the frequency calculation shows the structure to be a transition state (one imaginary frequency).

Table 8 summarizes and compares the calculated total energy, geometry (rotational constants) and dipole moment of the four different ozonides.

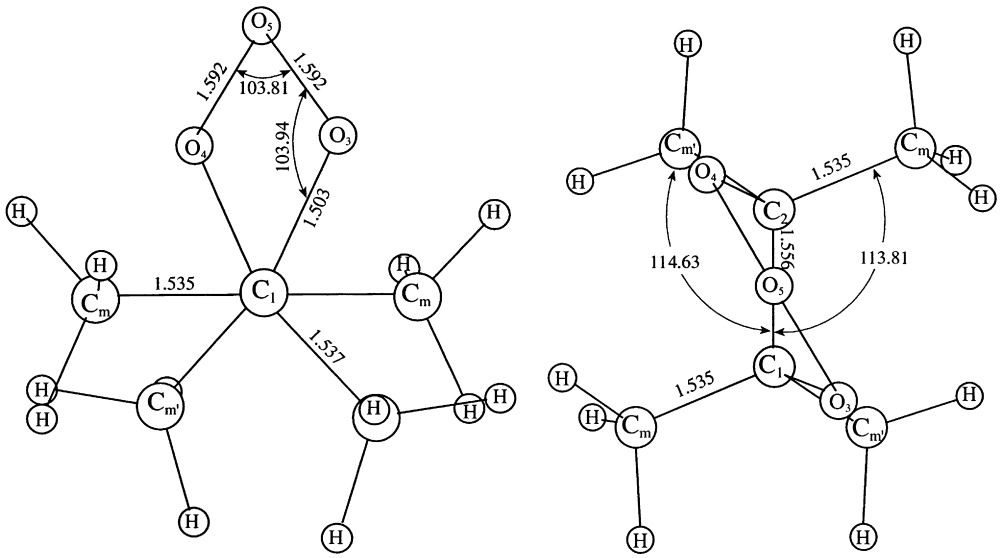

TMEPOZ CALCULATED GEOMETRY
SIDE VIEW

TMEPOZ CALCULATED GEOMETRY
TOP VIEW

Scheme 5. The calculated structure of the primary ozonide of tetramethylethylene.

Table 4
The experimental and calculated vibrational frequencies of HSOZ

Exp. frequency[a] gas phase (cm^{-1})	Intensity[a] (a.u.)	Exp. frequency[b] neat film (cm^{-1})	Intensity[b] (a.u.)	Calc. frequency[c] (cm^{-1})	Intensity (a.u.)
		688	3	704	1.1
		730	5	711	2.9
		736	2	733	1.8
				772	6.8
		824	7	823	8.4
				846	4.5
		887	3	867	11.9
				894	3.3
		934	20	947	18.4
		942	6	967	58.6
		970	17	984	3.2
984	32	982	44	1023	45.0
		1000	8	1026	3.2
		1016	5		
1065	76	1055	43	1073	184.7
		1063	11		
1107	100	1104	100	1092	34.6
		1120	27	1118	9.2
		1137	11	1129	5.9
		1153	1	1192	2.3
1209	5	1208	6	1203	1.9
		1220	8	1227	0.4
		1249	4	1264	3.9
		1287	3	1280	1.5
				1298	1.0
				1311	1.0
				1354	7.8
1325	9	1340	8	1359	25.8
1390	29	1379	19	1367	12.4
		1400	4	1374	13.9
		1414	1	1437	4.0
				1446	0.5
				1457	0.7
				1459	8.9
1466	15	1470	72	1470	10.0
				1476	1.0
2890	104	2861	59	2887	8.3
		2871	26	2896	38.0
		2928	195	2902	107.0
				2908	38.1
				2914	12.4
				2918	26.4
				2932	23.3
				2942	13.1
				2964	6.4
2967	122	2955	193	2968	115.0
				2969	56.0
				2998	21.0

[a]Experimental vibrational frequencies in the gas phase [16], intensities normalized to the strongest band at the finger print region (1107 cm^{-1}).

[b]Experimental vibrational frequencies in a neat film—this work. Intensities determined from the area of the vibrational bands in a neat film, and normalized to the strongest band in the finger print area. Similar to the HPOZ results, Table 3, the bands in the 2800–3000 cm^{-1} region of the experimental spectra are wide and overlap causing significant uncertainty in the determination of the area of individual bands.

[c]Calculated vibrational frequencies, (B3LYP/6-311G*, factor of 0.9613).

5. Discussion

5.1. Comparison with ethylene ozonation

The results of TME and 1-hexene ozonation in an amorphous CO_2 matrix are in good qualitative agreement with the previous findings for ethylene [5]. Both TME and 1-hexene react with ozone at a very low temperature (25–26 K) in amorphous CO_2. The appearance of the POZ and SOZ in the case of

Table 5
The experimental and calculated vibrational frequencies of TMEPOZ

Exp. frequency[a] (cm^{-1})	Exp. frequency[b] (cm^{-1})	Exp. intensity[b] (a.u.)	Calc. frequency[c] (cm^{-1})	Calc. intensity[c] (km/mol)
	576	2	576	4.33
	650	12	611	0.43
	668	1	635	12.09
682	691	15	674	5.38
721	729	100	757	11.28
	843	9	790	8.85
852	854	25	880	1.47
953	950	10	924	0.43
			926	0.22
			927	0.35
			993	0.25
	1095	6	1003	0.11
	1142	35	1136	14.22
1148	1146	95	1149	27.40
	1152	27	1164	30.47
1197	1196	25	1193	6.15
			1219	0.20
	1261	8	1249	1.90
			1368	2.71
1370	1394	28	1370	22.89
			1382	16.76
			1390	6.98
			1448	0.83
			1452	2.47
			1454	9.64
			1463	1.69
			1470	7.49
			1473	10.13
			1477	5.69
	1482	8	1482	10.67
			2866	1.93
			2867	5.98
			2869	16.73
			2871	20.41
			2944	2.60
			2945	2.04
			2949	35.79
			2950	21.41
			2974	2.83
			2975	10.99
			2976	2.20
			2976	21.18

[a]Experimental vibrational frequencies in a neat film at 88 K [10].

[b]In an argon matrix, at 37 K. Intensities are derived from the area of each peak. Note that at the 2800–3000 cm^{-1} region TMEPOZ bands are overlapped by TME bands.

[c]Calculated vibrational frequencies (MP2/6-31G, factor of 0.9338).

1-hexene is simultaneous, as found for the ozonation of ethylene, thus supporting the need to modify the Criegee mechanism as suggested in our previous work [5]. A possible explanation for the reactivity in the amorphous CO_2 (compared to the lack of reactivity, for ethylene and 1-hexene, in the argon matrix) is its considerably porous structure. Such a structure is likely to contain spacious trapping sites that do not hinder the molecular rearrangements, required during the ozonation reaction, contrary to the restrictions imposed by the rigid trapping sites in an argon matrix [5]. However, this explanation does not account for the onset of the reaction at a very low temperature (26 K), considering the high gas-phase activation energy (~5 kcal/mol for ethylene [9]). From Table 1 it is evident that at 26 K practically no reaction should

Table 6
The experimental and calculated vibrational frequencies of TMESOZ

Exp. frequency[a] (cm^{-1})	Exp. intensity[a] (a.u.)	Calc. frequency[b] (cm^{-1})	Calc. intensity[b] (km/mol)
845	0.4	821	10.6
860	0.2	827	30.6
876	0.3	868	0.3
		898	2.7
		901	0.8
		932	0.8
1005	1.0	971	117.7
		977	0.5
		978	0.2
1115	0.2	1094	8.3
1215	1.4	1180	253.7
		1191	1.9
1245	0.6	1192	48.4
1265	0.3	1213	69.7
		1233	5.9
		1355	0.9
1375	0.9	1357	59.5
		1368	30.9
		1372	2.5
		1432	0.0
		1435	0.0
		1436	2.7
		1448	0.5
		1434	0.7
		1453	0.1
		1455	1.8
1470	0.2	1461	16.5
		2926	0.0
		2926	22.6
2940	0.4	2933	25.9
		2934	0.9
		2989	5.0
		2989	5.0
		3000	9.8
3000	0.6	3000	48.3
		3009	4.5
		3010	32.3
		3013	37.6
		3013	1.7

[a]Experimental vibrational frequencies [23]. Intensity was estimated from a transmittance spectra [23].
[b]Calculated vibrational frequencies, (B3LYP/6-311G*, factor of 0.9613).

be observable for ethylene and other small unbranched olefins (though it is feasible for TME). The reactivity of ethylene at 26 K could be explained were the activation energy in the matrix lower than the gas phase one. However, since in crystalline CO_2 the reaction occurs only above 77 K, the lowering of the activation energy must be related not only to the chemical nature of CO_2, but also to the amorphous matrix structure. The amorphous matrix is known to be porous, having a very large surface area as found from H_2 absorption experiments [6,27] which maximizes at deposition temperature of 20 K [27]. Thus, it could be suggested that there may be a surface effect stabilizing the transition state that catalyzes the reaction, owing to the unsymmetrical nature of a surface and to the large quadruple moment of CO_2 (1.43×10^{-39} Å/s/m^2 [37]). However, no other examples of catalysis by a CO_2 solvent were reported, making this option extremely unlikely.

Another suggestion is that for specific reactions the activation energy in the matrix may be lower than in the gas phase one. Pimentel et al. [38,39] examined the kinetics of the oxidation of NO to NO_2 by O_3 in nitrogen matrices. Even though the gas-phase activation energy is at least 10 kJ/mol (2.4 kcal/mol) a reaction was found to occur at the temperature range 12–20 K (activation energy determined to be 443 J/mol). Furthermore, for the ozonation of *cis*-2-butene and *trans*-2-butene in a krypton matrix Pimentel and Singmaster [12] reported values for the activation energy which were on the low end range of the gas-phase measured values. This led the authors to make the following statement: ''That raises the interesting question of whether the gas-phase value is an average of all collision geometries whereas in the carefully prepared matrix all of the geometries are the same and that this preferred geometry happens to be optimum for the ozonolysis reactions.'' [12]. It is interesting to note that for the ozonation of ethylene the lower range value of the activation energy determined in a crystalline CO_2 matrix (3–5 kcal/mol) was again lower than the gas-phase value (4.7 kcal/mol) [40,7]. However, even a value of 3 kcal/mol seems too high to allow a reaction at 26 K. Moreover, Pimentel's

Table 7
The calculated dipole moment and geometry of TMEPOZ

	MP216-31G	MP214-31G	AM1	HP4-31G
Dipole moment (Debye)	5.24	5.20		5.04
Rotational constants (MHz)				
A	1825.50	1833.40	1948.74	1913.22
B	1723.59	1733.47	1760.01	1769.07
C	1451.48	1458.32	1509.20	1509.02
Bondlengths (Å)				
r (C_1–O_3)	1.503	1.500	1.480	1.464
r (C_1–C_2)	1.556	1.552	1.562	1.543
r (C_3–O_5)	1.592	1.591	1.303	1.469
r (C_m–C)	1.535	1.531	1.514	1.521
r ($C_{m'}$–O)	1.537	1.533	1.514	1.518
Bond angle (°)				
$C_1C_2O_4$	101.62	101.58	100.64	100.27
$C_1O_3O_5$	103.94	103.76	107.99	106.35
$O_3O_5O_4$	103.81	103.80	108.05	105.78
$C_1C_2C_m$	113.81	113.84	114.61	113.83
$C_1C_2C_{m'}$	114.63	114.61	114.61	115.49
Dihedral angle (°)				
$C_1O_3O_4C_2$	326.99	326.73	0.00	329.37
$C_mC_1C_2C_{m'}$	313.94	313.35	0.00[a]	317.06
Energy (h)	–459.3470558	–458.8867553		–457.9244513

Atom numbering correspond to the geometry of TMEPOZ as depicted in Scheme 5.

C_m stands for carbon of a methyl. Owing to the symmetry of the molecule, of the four methyl groups there are only two types: C_m and $C_{m'}$.

[a]For the AM1 calculated TMEPOZ which is of C_S symmetry the relevant angle for comparison is C_mCCC_m.

suggestion calls for a carefully prepared matrix generating the optimal geometry for a reaction, whereas an amorphous CO_2 matrix is not likely to contain only one optimal site geometry but rather a distribution of sites.

Another possibility is that the activation energies derived for the ozonolysis reaction at high temperatures (Table 1 and Ref. [9]) are not relevant at cryogenic temperatures. When the activation energies are small (as is the case for the ozonolysis reaction) the assumption that temperature dependence of the preexponential factor in the Arrhenius expression is negligible is no longer valid. Thus, for a bimolecular reaction with zero activation energy, the gas kinetic collision frequency increases with the square root of the temperature, leading to a larger rate constant. In a limited temperature range, of say 280–370 K, this increase may be erroneously interpreted as an activation energy of ~2 kcal/mol. It is interesting to note that another olefin, *trans*-2-butene is also reported to react at cryogenic matrices already at 25 K [41], whereas if the high-temperature derived activation energy (2.3 kcal/mol) is to be used a negligible rate constant is expected (Table 1). Similarly, 1-propene is reported in the same paper to react already at 50 K—a temperature much too low if the literature activation energy is to be used. These results support the notion that the high-temperature Arrhenius parameters are not applicable at cryogenic temperatures.

It is proposed that the ozonation reaction at the low temperature of 26 K in amorphous CO_2 matrix is related to the phase transition (crystallization process). It is noted that in all cases where ozonation commenced in amorphous CO_2 matrices there was a concomitant decrease in the CO_2 forbidden molecular transitions (ν_+ and ν_-). This decrease is thought to originate from a crystallization process that the amorphous system undergoes in the temperature range of 25–55 K [24]. This effect was noted also in pure CO_2 solids when no reaction was involved (see Fig. 3). The connection between the reaction and the crystallization may not be coincidental. A previous study of solid CO_2 [27] noted that at low deposition temperatures (the effect maximizing at 20 K according to adsorption measurements) an increasing part of CO_2 molecules form a metastable phase, being extremely unstable against temperature perturbations. Under these conditions considerable amounts of energy (estimated as 1% of the condensation energy) were released upon structural changes (phase changes). It was postulated that this metastable phase is formed when the CO_2 molecules aligned with each other in parallel. This energy release, however, cannot be used to overcome the room temperature estimated barrier, as the following rough estimate shows. The condensation energy (which is equal to the enthalpy of evaporation) is 70 cal/g (3.08 kcal/mol) at -30°C [42]. If the crystallization energy released is indeed about 1%, it will amount to about 31 cal/mol. This is much too small for the ethylene reaction to take place unless some kind of energy pooling occurs.

The crystalIization process is accompanied by geometry changes that may reduce environmental structural restrictions on the reaction. Although it ultimately leads to the creation of a more organized and a more tightly stacked solid (a crystal), the formation of the CO_2 crystal may eject the ethylene–ozone pair out into spaces in between crystallites. Some experimental data seem to support this suggestion. In particular, it rationalizes the fact that for all olefins studied (ethylene, 1-hexene, TME) the threshold temperature for a reaction in amorphous CO_2 was about 26 K, even though the activation energies that apply to these different olefins vary considerably. If

Table 8
Calculated properties of TME and 1-hexene primary and secondary ozonides

Ozonide		HPOZ	HSOZ	TMEPOZ	TMESOZ
Level		B3LYP/6-311G*	B3LYP/6-311G*	MP2/6-31G	B3LYP/6-311G*
Energy		–461.5673947	–461.5445300	–459.3470588	–461.5673947
Rot. Const. (MHz)	A	5139.00	4502.82	1825.50	2719.92
	B	618.72	679.62	1723.59	1386.66
	C	580.87	646.73	1451.48	1260.63
Dipole moment (Debye)		3.89	1.31	5.24	1.40

the reaction is initiated by the crystallization process then indeed the threshold temperature should be independent of the nature of the olefin. Our experiments with pure amnorphous CO_2 matrices (or with only one of the reactants) show that indeed the crystallization process starts at 26 K.

5.2. Mixed matrices

The composition of mixed matrices was studied by various methods, including neutron inelastic scattering and X-ray diffraction, using both low mixing ratios (less than 5%) and up to complete mixing (a 1:1 mixture) [43–45]. Molecular dynamics based computer simulations helped to estimate the structure of these complex systems [46,45]. Guests trapped in these matrices may be found either in an environment of one of the pure components (poor mixing) or in a site formed by both (strong mixing).

CO_2/Kr mixed matrices were studied recently by X-ray diffraction and IR [45], showing that using regular codeposition from the gas phase, phase separation occurred, presumably by diffusion during deposition. A homogeneously mixed solid of CO_2 and Kr formed only upon increasing the cooling efficiency during deposition by using a helium flow. In the concentration range of 30–70 mol% Kr the resultant solid was amorphous. MD simulations support this finding and imply that it is owing to internal distortions (orientational and center of gravity disorder) rather than to grain size effects [45].

The nature of the Ar/CO_2 mixed matrices prepared in this work (homogenous mixture or phase separation) was probed by considering changes in the IR spectrum of ozone and ethylene. In the 1:1 Ar/CO_2 mixture two IR bands owing to the ν_3 ozone mode were found: a dominant one having the typical frequency of ozone in pure argon matrix (1038.3 cm^{-1}) and the smaller one (about 1/7 in area) having the typical frequency of ozone in a pure CO_2 matrix (see Fig. 7). This may imply that the resultant matrix is predominantly composed of two separate phases, with the ozone concentrated mostly in the argon one. The relatively large width of the ozone bands indicates that this separation is not complete, but some minor mixing between the phases does occur. The spectrum of ethylene in the 1:1 Ar/CO_2 mixture also shows one major band and one minor band (960.7 and 947 cm^{-1}, respectively, see Fig. 7). The latter is the same as Ethylene's band in argon, indicating that a small part of the ethylene resides in a pure argon phase. (This is also the frequency of the minor band of ethylene in a CO_2 matrix, but the frequency of the stronger band the 969.5 is missing, thus ruling out this interpretation.) The major band at 960.7 cm^{-1}, however, is not characteristic for ethylene in a CO_2 matrix, indicating that the majority of the ethylene molecules are not residing separately in an argon or CO_2 phase. They appear to occupy interfacial sites in between microcrystallites, or in a mixed phase. Thus, the 1:1 mixed matrix exhibits some phase separation, but also selective trapping of the two reactants, effectively decreasing the chances for ozone–ethylene adduct formation and consequently of the reaction probability. Indeed, no reaction was observed in the 1:1 Ar/CO_2 mixture. Additional experiments that included only one reactant revealed that the distribution of each reactant among the two phases as determined from the vibrational IR bands, was not affected by the presence of the other. In this mixed matrix, even though a separate CO_2 phase seems to be formed and ν_+/ν_- bands associated with the amorphous phase are present, no indication for a crystallization process could be observed upon heating to 26 K or even to 35 K. It is possible that the cooperative crystallization process is hindered by the presence of the argon impurity.

The ozone bands in the 1:9 Ar/CO_2 mixture indicate that ozone is located primarily in a CO_2 phase. The ethylene spectra are more complicated, indicating that these molecules 'prefer' to reside in a CO_2 phase, though a considerable fraction occupy sites in between the phases, or in a mixed trapping site. Heating the matrix to 26 K leads to a decrease in ν_+/ν_- band intensity and to the initiation of a reaction (Fig. 8).

Thus, the results of experiments in Ar/CO_2 mixed matrices agree with the suggested reaction model, showing again that when crystallization is hindered there is no reaction and that the phase transition initiated at 26 K occurs concurrently with the reaction.

5.3. The reaction temperature dependence

Another support for the close relationship between the crystallization process and the ozonation reaction

arises from the difference between the temperature dependence of reaction yield in CO_2 versus the argon matrices. For the TME–ozone system in an amorphous CO_2 matrix, once the product bands reached a plateau (at 26 K), heating the matrix to higher temperatures did not generate any further product. It appears that the reaction at that low temperature exhausted the reactivity potential of the matrix. In contrast, ozonation of TME in argon displayed a different temperature–time behavior the product bands reached a plateau at a given temperature with time, as in the CO_2 matrix. However, further temperature rise led to a pronounced increase in product absorption peaks (see Fig. 4). This pattern is expected for a matrix containing several sites with varying geometries, resulting with reactant pairs with different activation energies. The different activation barriers may relate to orientational changes within the trapping sites. Since in the amorphous CO_2 matrix this pattern is not found, site distinction does not affect the reaction rate, as expected if the main effect is owing to long range phase changes.

In particular, extensive product formation was observed at 40 K, a temperature at which the matrix is still intact, though much more flexible than at 35 K. It is clear that the 'softening' of the matrix is related to the onset of a rapid reaction. The simplest interpretation is that TME and ozone are able to approach each other at this temperature by diffusion and, being free from spatial restrictions, proceed to react. This pattern was found also for ethylene [5] at the same temperature, in spite of the large difference between the high-temperature activation energies of these two reactions (Table 1).

The codeposition experiment, in which TME and ethylene were deposited together in an amorphous CO_2 matrix, provides further insight to the reaction mechanism. It was found that the onset temperature of the products appearance was practically identical for the two olefins. The rate of TME ozonation was about 30 times faster than that of ethylene, while the rate constant were practically the same (Section 3.4). The most plausible explanation of this result is that the concentration of TME–ozone pairs in the matrix is much larger than that of the ethylene-ozone pairs. This would be the expected trend in thermodynamic equilibrium, as the van der Waals binding energy of ozone to TME is expected to be much larger than that of ethylene. This is owing to the larger size of TME, and also to the increased electron density on the double bond, acting to bind better to the electrophilic ozone.

6. Molecular simulations

In an attempt to rationalize the reactivity pattern observed for TME in argon, molecular dynamics (MD) simulations [31] of the trapping sites of TME–ozone pairs and of the product TMEPOZ were carried out. Such simulations [5] indicated that ethylene ozonation in an argon matrix is unlikely: all calculated trapping sites containing an ethylene–ozone pair were found to be unable to accommodate EPOZ. Rather, the calculated site of EPOZ was larger in volume than that of any site of ethylene–ozone pair, predicting that no reaction will take place in argon, as found experimentally. In the present simulations, as in the case of the ethylene–ozone pair, the molecules were treated as rigid bodies, using the quantum chemical calculated structure (Section 4.1.2).

The TME–ozone pair was found to be trapped predominantly in five or six substitution sites. In both, the argon atoms were replaced in two adjacent 100 planes. As an example, Fig. 10 shows the MD calculated six substitutional site of the TME–ozone pair in an argon matrix. For clarity, Fig. 10(a) shows one 100 plane from which argon atoms are replaced, and Fig. 10(b) the adjacent one. In the former the ozone molecule is seen to replace two argon atoms and one more argon atom is considerably displaced from its original position. In the other, TME replaces four argon atoms.

The ozonation product TMEPOZ was also calculated to occupy either a five or a six substitution sites, again in two adjacent 100 planes. Fig. 11 shows a MD calculated five substitution site of the TMEPOZ in an argon matrix. Like the TME–ozone pair, the ozonide is also found in two adjacent 100 planes. Two argon atoms are replaced in one 100 plane and three in the other.

Comparison of the calculated site structures of the ozone–TME pair with that of the TMEPOZ shows the TME–ozone sites can easily accommodate the product. In sharp contrast to the ethylene–ozone case, there is no obvious spatial hindrance for the reaction of the ozone

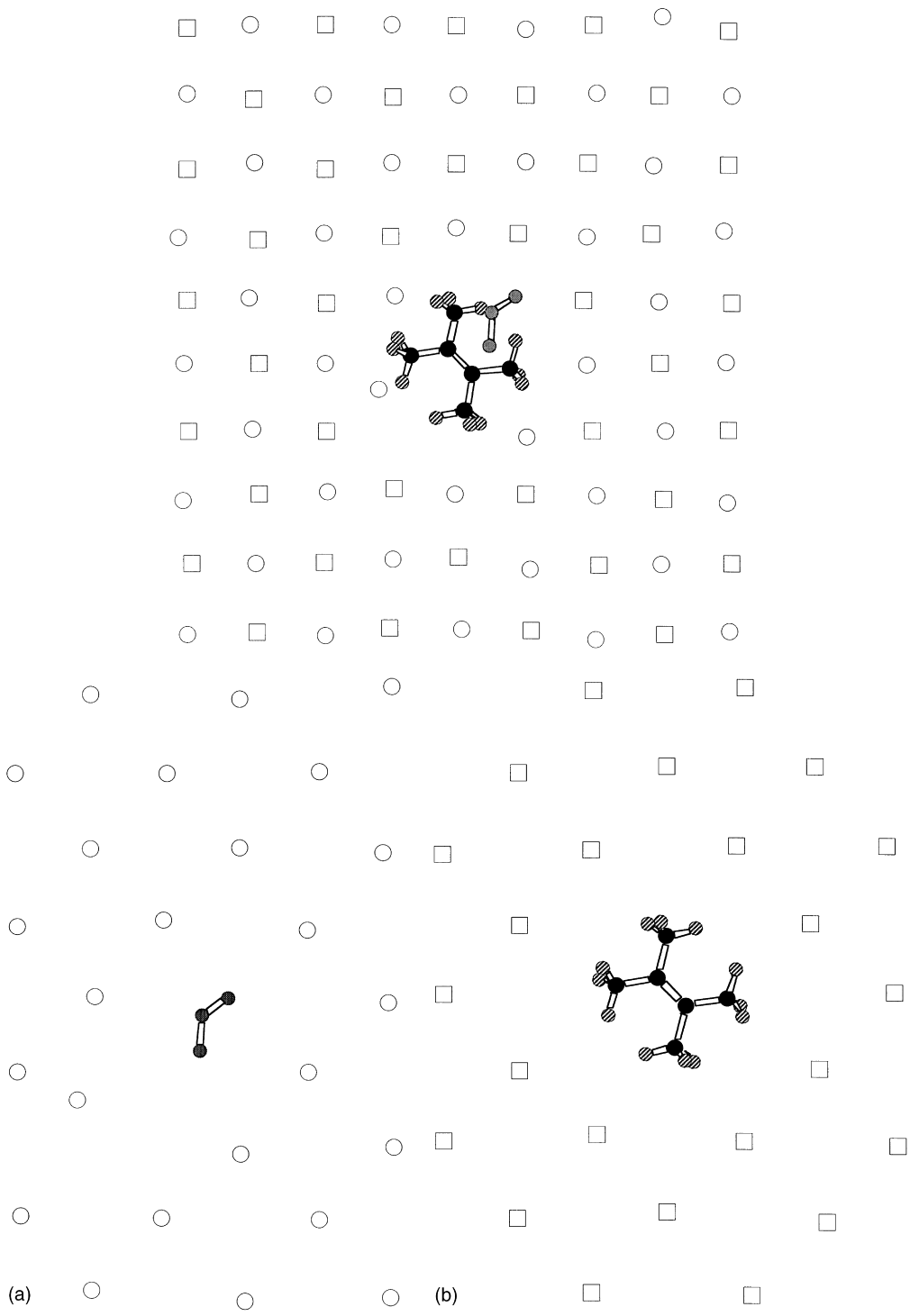

Fig. 10. MD calculated, six substitution site of the ozone–TME pair, in an argon matrix. The figure displays two 100 planes. The argon atoms constituting the top 100 argon plane are represented by open circles and the argon atoms constituting the lower 100 argon plane by open squares. Carbon atoms are black, ozone atoms gray and hydrogen atoms are marked by black and white stripes. (a) The upper 100 plane; (b) the lower 100 plane.

and TME pair to form the TMEPOZ in an argon matrix. For example, the six-substitution trapping site of the ozone–TME adduct shown in Fig. 10 is similar in structure to that of the product's, the TMEPOZ site, shown in Fig. 11. Moreover, the site occupied by the ozonide product is smaller implying that there is enough room in the pair site to allow it to form the ozonide product.

For a reaction to be feasible the ozone and TME molecules must be situated in the proper relative orientation that allows the formation of the product TMEPOZ. Many of the pair's calculated sites do not conform with this criteria, but some do (such one site was shown above). Thus, the simulation predicts that some of the ozone–TME adduct sites will allow a reaction in argon, as found experimentally. Moreover, since the trapping sites of the ozone–TME pair are found to be fairly spacious, the temperature–time pattern discussed in Section 5.3 can be qualitatively accounted for. At low temperatures, only those pairs that are found in a favorable orientation will react. Other trapping sites remain inert, even though they contain the two reactants in close proximity. Raising the temperature induces thermal motion that leads to the proper orientation for reaction in additional sites.

7. Summary

It is found that the ozonation of both TME and 1-hexene takes place at the low temperature of 26 K in an amorphous CO_2 matrix. (In line with our previous findings for ethylene.) The pseudo first order rate constant for ethylene and TME is essentially the same, even though the high-temperature activation energy for ethylene is much larger than for TME. At 26 K, amorphous CO_2 undergoes a phase transition to a crystalline phase; it is suggested that this macroscopic cooperative change allows the re-orientation of the reactants, and thus enables their reaction. In a crystalline argon matrix, ethylene and 1-hexene remain inactive up to the softening temperature of this crystalline matrix. This was previously found to be consistent with molecular dynamics (MD) simulations on ethylene–ozone deposition in argon [5]—the two

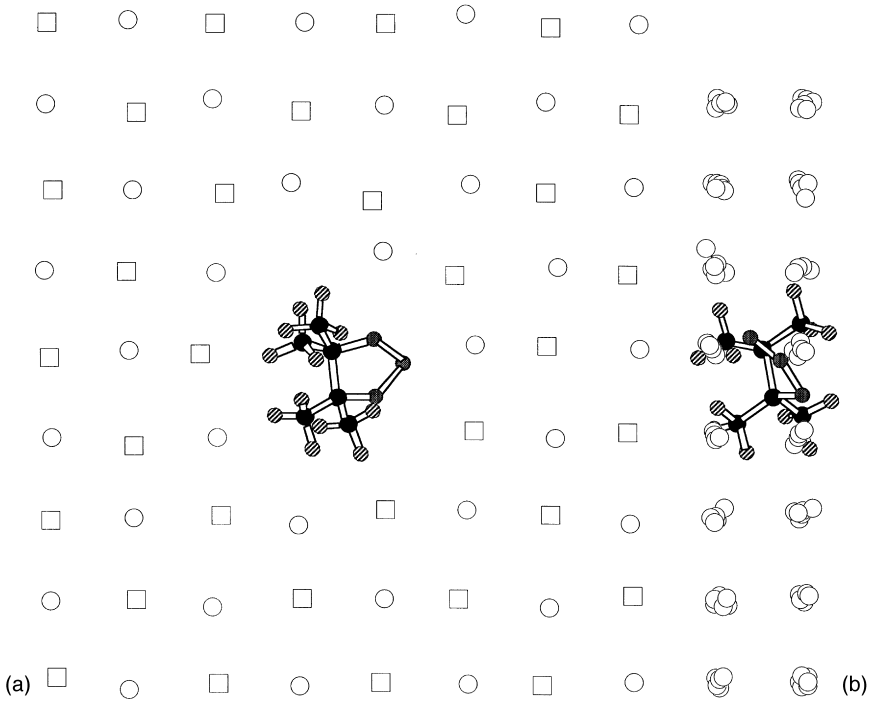

Fig. 11. MD calculated, five substitution site of TMEPOZ in an argon matrix. Like the ozone–TME pair, the ozonide is also trapped in two adjacent 100 planes. Two argon atoms are missing in the upper 100 plane and three in the lower 100 plane. (a) and (b) show a top and side view of the same site.

reactants were found to be trapped in a configuration that does not enable the formation of the primary ozonide. In contrast, MD simulations of the TME–ozone pair show that deposition in argon leads to trapping sites capable of supporting the reaction. The temperature dependence of the reaction rate is interpreted as showing that intra-site reorientation is needed for the reaction to proceed. An attempt to overcome the mechanical fragility of the amorphous CO_2 matrix through the use of argon/CO_2 mixed matrices showed that a reaction commenced only when CO_2 percentage was 90%. The absence of reaction in the mixed matrices (argon percentage being larger than 10%) is attributed to the absence of CO_2 crystallization under these conditions and to limited number of reactant pairs formed owing to phase separation.

It is concluded that in both argon and CO_2 matrices, the addition of ozone to the olefins takes place even at very low temperatures, provided the pairs can attain the necessary relative orientation. This implies that the high-temperature activation energy, which was reported to be as high as 5 kcal/mol in the case of ethylene, is irrelevant to the matrix studies.

Quantum chemical calculations of the structures and IR spectra of the primary and secondary ozonides of 1-hexene and TME are reported. The calculated spectra are in reasonable agreement with the experimental ones. The calculated structures were used in the MD simulations of the trapping in solid argon.

Acknowledgements

This research was supported under grant no. HRN-2078, C12-223, US–Israel Cooperative Development Research Progrwn, Office of the Science Advisor, US Agency for International Development. The Farkas Center is supported by Minerva mbH, Munich. We thank Professor K. Griesbaurn for useful correspondence and for reporting some of his data prior to publication.

References

[1] R. Criegee, Rec. Chem. Prog. 18 (1957) 111.
[2] R. Kuczkowski, Chem. Soc. Rev. 21 (1992) 79–83.
[3] D. Cremer, E. Kraka, M.L. McKee, T.P. Radhakrishnan, Chem. Phys. Lett. 187 (1991) 491.
[4] R. Ponec, G. Yuzhakov, Y. Haas, U. Samuni, J. Org. Chem. 62 (1997) 2757–2762.
[5] U. Samuni, R. Fraenkel, Y. Haas, R. Fajgar, J. Pola, J. Am. Chem. Soc. 118 (1996) 3687.
[6] E. Knözinger, W. Schuller, W. Langel, J. Phys. Chem. 97 (1993) 927.
[7] W.B. DeMore, Int. J. Chem. Kin. 1 (1969) 209.
[8] K.H. Becker, U. Schurath, H. Seitz, Int. J. Chem. Kin. 6 (1974) 725.
[9] R. Atkinson, W.P.L. Carter, Chem. Rev. 84 (1984) 437–470.
[10] L.A. Hull, I.C. Hisatsune, J. Heicklen, J. Am. Chem. Soc. 94 (1972) 4856–4864.
[11] B. Nelander, L. Nord, J. Am. Chem. Soc. 101 (1979) 3769.
[12] K.A. Singmaster, G.C. Pimentel, J. Phys. Chem. 94 (1990) 5226.
[13] H. Niki, P.D. Maker, C.M. Savage, L.P. Breitenbach, M.D. Hurley, J. Phys. Chem. 91 (1987) 941–946.
[14] R.I. Martinez, J.T. Herron, J. Phys. Chem. 91 (1987) 946–953.
[15] D. Grosjean, E. Grosjean, E.L. Williams II, Environ. Sci. Tech. 28 (1994) 186–196.
[16] R. Fajgar, J. Vitek, Y. Haas, J. Pola, J. Am. Chem. Soc., submitted.
[17] S.D. Razumovskii, L.V. Berezova, Izvest. Akad. Nauk S.S.S.R., Sov. Chim. 1 (1968) 207.
[18] N.I. Boldenkov, S.D. Razumovskii, Khim. Prom-st. 2 (1977) 100–103.
[19] B. Mile, G.W Morris, W.G. Alcock, J. Chem. Soc., Perkin II, 1644 (1979).
[20] P.S. Bailey, Ozonation in Organic Chemsitry, vol. 1, Academic Press, New York, 1978.
[21] P.S. Bailey, Chem. Rev. 58 (1958) 925.
[22] K. Griesbaum, W. Volpp, R. Greinert, J. Am. Chem. Soc. 107 (1985) 5309.
[23] K. Griesbaum, W. Volpp, R. Greinert, H.J. Greunig, J. Schmid, H. Henke, J. Org. Chem. 54 (1989) 383–389; and private correspondence.
[24] M. Falk, P.F. Seto, Can. J. Spectrosc. 31 (1986) 134.
[25] M. Falk, Can. J. Chem. Phys. 86 (1987) 560.
[26] H.L. Löwen, K.D. Bier, H.J. Jodl, A. Löwenschuss, A. Givan, J. Chem. Phys. 90 (1989) 5309.
[27] W. Schulze, H. Abe, Chem. Phys. 52 (1980) 381–388.
[28] M.J. Frisch, G.W. Trucks, H.B. Schlegel, P.M.W. Gill, B.G. Johnson, M.A. Robb, J.R. Cheeseman, T. Keith, G.A. Petersson, J.A. Montgomery, K. Raghavachari, M.A. Al-Laham, V.G. Zakrzewski, J.V. Ortiz, J.B. Foresman, J. Cioslowski, B.B. Stefanov, A. Nanayakkara, M. Challacombe C.Y. Peng, P.Y. Ayala, W. Chen, M.W. Wong, J.L. Andres, E.S. Replogle, R. Gomperts, R.L. Martin, D.J. Fox, J.S. Binkley, D.J. Defrees, J. Baker, J.P. Stewart, M. Head-Gordon, C. Gonzalez, J.A. Pople, Gaussian 94, Revision DA, Gaussian, Inc., Pittsburgh, PA, 1995.
[29] W.J. Hehre, R. Ditchfield, J.A. Pople, J. Chem. Phys. 56 (1972) 2257.
[30] M.W. Wong, Chem. Phys. Lett. 256 (1996) 391–399.
[31] R. Fraenkel, Y. Haas, Chem. Phys. 186 (1994) 185.

[32] M.P. Allen, D.J. Tildesley, Computer Simulations of Liquids, Oxford University, New York, 1987.
[33] J.Z. Gillies, C.W. Gillies, R.D. Suenram, F.J. Lovas, J. Am. Chem. Soc. 110 (1988) 7991.
[34] U. Samuni, Y. Haas, Spectrochim. Acta. Part A 52 (1996) 1479–1492.
[35] C.W. Gillies, R.L. Kuczkowski, J. Am. Chem. Soc. 94 (1972) 6337, 7609.
[36] R. Latimer, R.L. Kticzkowski, C.W. Gillies, J. Am. Chem. Soc. 96 (1974) 348.
[37] C.S. Murthy, S.F. O'Shea, I.R. McDonald, Mol. Phys. 50 (1983) 531.
[38] D. Lucas, Ph.D. Dissertation, University of California, Berkeley, CA, 1976.
[39] G.C. Pimentel, Ber. Bunsenges. Phys. Chem. 82 (1978) 2–6.
[40] B. Nelander, L. Nord, Tetrahedron Lett. 32 (1977) 2821.
[41] I.L. Andrews, C.K. Kohlmiller, J. Phys. Chem. 86 (1982) 4548–4557.
[42] R.C. Weast, M.J. Astle (Eds.), CRC Handbook of Chemistry and Physics, 60th ed., CRC Press, Boca Raton, FL, 1979.
[43] W. Press, B. Janik, H. Grimm, Z. Phys. B, Condensed Matter 49 (1982) 9–16.
[44] W. Langel, A. Becker, H.W. Fleger, E. Knozinger, J. Mol. Struct. 297 (1993) 407–413.
[45] W. Langel, H.W. Fleger, E. Knozinger, W. Schuller, Ber. Bunsenges. Phys. Chem. 99 (1995) 940–950.
[46] S. Nose, M.L. Klein, Can. J. Phys. 60 (1982) 1365–1370.